Mixing properties of a stably stratified parallel shear layer

Paolo Monti[a)]
Dipartimento di Idraulica Trasporti e Strade, Università di Roma "La Sapienza", Roma, Italy

Giorgio Querzoli
Dipartimento di Ingegneria del Territorio, Università di Cagliari, Cagliari, Italy

Antonio Cenedese and Simonetta Piccinini
Dipartimento di Idraulica Trasporti e Strade, Università di Roma "La Sapienza", Roma, Italy

(Received 8 January 2007; accepted 28 May 2007; published online 21 August 2007)

The results of a laboratory investigation on turbulent mixing of mass and momentum associated with the collapse of Kelvin-Helmholtz waves which develop in a stably stratified parallel shear layer with $O(10^3)$ Schmidt number are presented. The waves were generated in a stratified, tilting tank using a denser fluid underlying a lighter fluid with a velocity shear between the layers. Detailed velocity and density measurements were conducted simultaneously using particle tracking velocimetry and laser-induced fluorescence techniques. Estimation of the efficiency of mixing, the ratio between the diffusive flux of density responsible for mixing, to the turbulent kinetic energy dissipation rate, suggest it is independent of the initial values of the Reynolds and the bulk Richardson numbers. The measurements of the eddy diffusivities of mass and momentum showed a reasonable agreement with other laboratory-based predictions of turbulent mixing and observational data in atmospheric stably stratified flows. © *2007 American Institute of Physics*.
[DOI: 10.1063/1.2756580]

I. INTRODUCTION

Turbulent mixing of stably stratified shear layers is of great importance in geophysical flows. The sheared thermocline in the oceans[1] and nocturnal atmospheric slope flows[2] are common cases in which mixing of momentum, heat, and mass play dominating roles in the dynamics of the flow. Since mixing occurs at the smallest scales of the flow at which molecular processes are acting, its estimation is rather complex. Much research effort over the past three decades has gone into the development of realistic parameterizations and modeling of the mixing properties of stably stratified shear layer flows. The variety of work on the turbulent mixing in stratified parallel flows has been ably summarized by Ref. 3.

Given its ubiquitous occurrence in stably stratified flows, Kelvin-Helmholtz (KH) instability represents a prototype for turbulence production in geophysical flows.[4,5] KH instability appears at the interface between two parallel streams of different velocities and densities (with the heavier fluid at the bottom) when the destabilizing effect induced by the velocity shear, which promotes turbulent production, overcomes the stabilizing one associated with the buoyancy forces. Commonly, "KH instability" is used to refer to the general case even where the variations of velocity and density are continuous and occur over a finite thickness.[6]

The linear theory of nonviscous, steady, stratified, parallel shear flows[7,8] shows that KH instability may develop if $\mathrm{Ri}_G < 1/4$ somewhere within the flow. Here, $\mathrm{Ri}_G = N^2/(\partial u_x/\partial z)^2$ is the gradient Richardson number, $N = \sqrt{(-g/\rho_0)(\partial\rho/\partial z)}$ is the buoyancy frequency, u_x is the horizontal velocity, ρ is the density, ρ_0 is the mean density of the fluid, g is the modulus of the acceleration due to the gravity, and z is the vertical coordinate. The KH instability manifests itself as sinusoidal perturbations of the interface during the first stage of its life; its nonlinear development gives rise to coherent billows which generate sharp density gradients (in oceans) or temperature gradients (in the atmosphere). Subsequently, they collapse to form turbulent patches which induce rapid fluid mixing. This point is of crucial interest in developing mixing parameterization for geophysical forecasting models in the case of stably stratified flows.[9,10]

While the numerical approach has been extensively used to analyze the full life cycle of KH billows,[3] laboratory investigations have encountered strong limitations in the past, because of the difficulties related to the experimental setup. For example, the refractive index variations which arise from density differences within the fluid mixtures create distortions in the optical path, causing serious restrictions both for qualitative and quantitative flow visualizations. This problem has been overcome by the use of refractive index matching technique, in which fluids of different density but equal refractive index are used.[11] This method makes possible the exploration of the general characteristics of the KH instability via quantitative density measurements through the laser-induced fluorescence (LIF) technique.[12,13]

Another difficulty in using the experimental approach comes from the need for information about the velocity field over a large portion of the flow, that is, the whole area relevant to the KH billow. In fact, if the goal is to understand

[a)]Author to whom correspondence should be addressed: Università degli Studi di Roma "La Sapienza," Via Eudossiana, 18 00184 Roma, Italy. Electronic mail: paolo.monti@uniromal.it

the way in which a KH billow arises, grows, and collapses, it is apparent that standard acquisition methods like laser-Doppler or hot-film velocimetry are not well-suited in that they can give simultaneous information on the fluid velocity only in a limited number of points of the flow field (namely, only one for each probe). Conversely, particle tracking velocimetry (PTV) can measure the fluid velocity by tracking tracer particles mixed within the flow in a large portion of the field, without limitations linked to the intrusion of a probe which could alter significantly the measure.[14]

Velocity and density fields were measured simultaneously using an image acquisition system consisting of two cameras: the first one permitted the velocity field to be evaluated by PTV, while the second camera was used for the density measurement via LIF. Simultaneous measurements of velocity and density allowed the evaluation of important features such as the local gradient Richardson number and the mass flux.

On the basis of a standard analysis of a set of experiments, this paper is focused essentially on the mixing which develops once a KH billow collapses. The billows were generated using a tilting tank designed after that of Thorpe.[15] Details on the experimental methods are given in Sec. II. In Sec. III we briefly recall the main nondimensional governing parameters upon which the quantities of interest depend. Section III is also devoted to the analysis of the regimes that characterize the full life cycle of a KH billow, namely the phases of formation, growing, collapse, and subsequent relaminarization of the flow. We shall consider the way in which the eddy diffusivities of mass and momentum change in time and how the potential and the kinetic energy evolve during the different regimes. In addition, Sec. III reports the computation of the mixing efficiency Rf, defined as the ratio of the diffusive flux of density responsible for mixing (i.e., the irreversible increase of the potential energy of the density distribution associated with fluid mixing) to the irreversible loss of kinetic energy (see, for example, Refs. 16 and 17 for reviews). To this end, the theoretical development of Refs. 18 and 19 which provides an expression of the diffusive flux of density was used. In particular, we provided evidence that the asymptotic value of the mixing efficiency does not depend on the initial values of the Reynolds and the bulk Richardson numbers. Results are also discussed in comparison with direct numerical simulations found in the literature. Conclusions are drawn in Sec. IV.

II. EXPERIMENTAL SETUP

The experiments were performed using a Plexiglas tilting tank, 3700 mm long, 240 mm wide, and 22 mm deep (Fig. 1). It was initially horizontal and stably stratified with two fluids of equal depth ($H=11$ mm) and different densities. The tank, housed in a specially built steel structure to avoid any structural deformation during the experiments, was designed by Defina *et al.*[20] following the basic ideas given by Thorpe.[15] The stratification was obtained by filling the tank with its longest axis in the vertical direction using a peristaltic pump (in order to minimize heating of the fluids which can generate undesired density and refractive-index

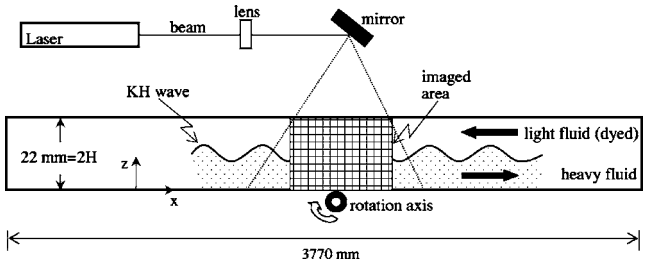

FIG. 1. The experimental setup (not to scale).

variations), and then, tilting it slowly to the horizontal position. The first half was filled with an aqueous ethanol solution (light fluid), whereas the second with a water-salt mixture (heavy fluid). The fluids for the two layers were prepared in separate tanks and a refractometer with an accuracy of 10^{-4} was used to measure the index of refraction. A thin, unavoidable, interfacial layer formed between the two fluids. The concentrations of both the mixtures were appropriate to set the desired density jump across the interface and, at the same time, match the index of refraction of the two layers to allow the quantitative flow visualization.

It is known that the mixing of aqueous ethanol and salt solutions having the same refractive index generates a new mixture with index of refraction slightly different from that of the original solutions. This variation, however, is very small and does not produce any significant distortions in the paths of the light rays.

The top light layer was premixed with a fluorescent dye (Sodium fluorescein). Nonbuoyant particles (pine pollen) were also dispersed in both the mixtures as tracer for the PTV analysis. The tilting of the tank from its horizontal position to a known angle, $\theta=6°$, provided the acceleration in opposite directions of the two layers. The ascending, upper-layer fluid and the descending, lower-layer fluid, generated at the interface a velocity shear which made the flow prone to the formation of a series of KH billows. Note that the billows are stationary with respect to the tank since the depth of the two fluids is the same. This fact permitted the billows to be monitored using fixed cameras.

The investigation area was rectangular ($\sim$100 mm $\times$22 mm), lying in the vertical center plane in the middle of the tank, and parallel to its longest axis. It was illuminated with a thin, argon-ion laser sheet. The area was large enough to include at least one KH billow, from its formation to the collapse. The laser was used in all-lines mode with a nominal power of about 300 mW. The aqueous ethanol solution, dyed with fluorescein, has a peak of absorption at about 514 nm and a peak of emission at about 540 nm. The emitted light was then captured by a digital CCD camera at 25 frames per second equipped with a filter to pass only the fluoresced light and cut-off the light emitted by the laser. The resolution of the camera was 512×720 pixels $\times$ 8-bit. The distribution of the light intensity in the framed area was measured by acquiring a reference image with a uniformly low concentration of fluorescein. Therefore, the intensity of the fluorescent light varied only because of the incident light. The dye concentration at a given pixel, which, in turn, was directly pro-

portional to the fractional volume of the dyed fluid, was assumed proportional to the luminosity measured during the experiment, normalized by the reference image at the same location. The method was calibrated by using the luminosity of the top (dyed) layer before mixing, as its density was known *a priori*. The fluorescein concentration was kept below a certain value in order to avoid nonlinearity between light intensity and dye concentration and minimize attenuation of the laser light as well. In any case, since the depth of the two layers was small, the attenuation of the laser light intensity due to the dye was negligible. Note that the use of the fluorescein as the marker for the stratifying scalar (density) is reasonable since fluorescein ($\mathrm{Sc}\approx 1000$) and salt ($\mathrm{Sc}\approx 700$) have similar Schmidt number, $\mathrm{Sc}=\nu/\kappa_\rho$, (where ν and κ_ρ are the kinematic viscosity and the molecular diffusivity of mass, respectively). Therefore, the concentration of the stratified scalar can be directly related to the optically measured dye concentration (see, for example, Ref. 13, and references therein).

Information about flow kinematics was extracted by using PTV, a nonintrusive technique based on the tracking of nonbuoyant seed particles. PTV is a reliable method that can yield very accurate, simultaneous velocity measurements over a wide area of a flow field. Among the previous applications, PTV has been successfully employed in laboratory studies of turbulent convection in the atmospheric boundary layer.[14] Particle images with a resolution of $1024\times 256\times 8$ bit were acquired at a rate of 250 per second by means of a high-speed, CMOS camera. The dimensions of the images were well-suited for the elongated shape of the interrogation area. The particles were identified by thresholding images after a dynamical background subtraction. Then, trajectories were reconstructed by connecting particles of successive frames according to the following criteria: (i) initial particle velocity cannot exceed a given value, (ii) particle acceleration must be less than an assigned value, and (iii) it is better to continue an existing trajectory rather than create a new one (the structure of the tracking algorithm is described in details in Ref. 14).

It must be noticed that the above thresholds (i) and (ii) are isotropic and therefore are perhaps not ideal for flow studied here, particularly during the first phase of motion, when both the velocity and the shear are very different in the horizontal and vertical directions. In fact, during that phase, the flow was still laminar and essentially directed along the axis of the channel, whereas velocity gradients were mainly vertical. To make the apparent motion more suitable for the above described analysis, all frames were stretched 3 times along the transversal direction by linear interpolation. That procedure has two beneficial effects. First, the transversal resolution in the determination of particle locations, and in turn the accuracy of the corresponding component of velocity, is increased (this is particularly meaningful when transversal velocities are small). Secondly, particles appear farther from each other, thus fewer ambiguities occur during trajectory recognition [i.e., it is less probable that two or more particles match the criteria (i)-(iii) at the same time for the same trajectory]. Velocity and acceleration thresholds have been tuned for each run of the experiment to be as low as possible, but high enough to not cut-off any realistic displacement of the particles. The information on the fluid density, obtained from the filtered camera, was spatially related to the velocity field obtained from the high-speed camera by a registration procedure. Two simultaneous images of stationary particles, dispersed within a stationary fluid, were acquired by the two cameras. Particle positions were computed on the two images and the affine transformation that best mapped the particles viewed from the filtered camera on those recognized by the high-speed camera was found by minimizing the mean square error. This transformation was used to map the density field onto the velocity field.

Note that, given the difference in the frame rate between the two cameras, the computation of the velocity field was based on a time interval equal to 25^{-1} s (corresponding to 10 frames of the high-speed camera). In so doing, both the density and the velocity fields subject of the following analysis will refer to the same sampling frequency of 25 Hz.

III. RESULTS AND DISCUSSIONS

A. Governing parameters

Dimensional analysis reported by several authors (see Ref. 20, among others) shows that the flow depends on three parameters: the Schmidt number, the gradient Richardson number calculated at the density interface ($z=H$):

$$\mathrm{Ri}_G\big|_{z=H}=\frac{g}{\rho_0}\frac{-\left.\frac{\partial\rho}{\partial z}\right|_{z=H}}{\left(\left.\frac{\partial u_x}{\partial z}\right|_{z=H}\right)^2} \tag{1}$$

and the overall Reynolds number,

$$\mathrm{Re}=\frac{\Delta U H}{\nu}, \tag{2}$$

where u_x is the longitudinal velocity component and ΔU is the maximum difference between the upper and the lower longitudinal velocity [in practice, the velocity difference between the two layers at the onset of the instability was used in Eq. (2)]. For sake of simplicity, hereinafter the gradient Richardson number will be implicitly considered to be computed at the interface and the symbol $|_{z=H}$ will be omitted. The angle of tilting $\theta=6°$ was adopted for all the experiments. This value was sufficiently large to attain the condition $\mathrm{Ri}_G<0.25$ within the flow.

For the present study, a series of about 60 experiments were performed and 4 of these were considered suitable for the current investigation. Their main parameters are listed in

TABLE I. Parameters of the experiments.

Expt #	$\Delta\rho(g1^{-1})$	Ri_B	Re
1	15	0.108	1348
2	22	0.092	1760
3	30	0.075	2273
4	38	0.084	2428
5	54	0.074	3080

Table I, together with the values of the bulk Richardson number,

$$\mathrm{Ri}_B = g\frac{\Delta\rho}{\rho_0}\frac{H}{(\Delta U)^2}, \tag{3}$$

$\Delta\rho$ being the density difference between the two layers at the start of the experiment.

B. The initial parallel flow

Before proceeding with the investigation of the turbulent mixing, it is useful to analyze the main features of the fully developed parallel shear flow prior to the onset of instability. The maximum longitudinal velocity u_x was in the interval 50–120 mm s^{-1} during most of the experiments. Correspondingly the Reynolds number ranged from ~1000 to ~3000, while the bulk Richardson number was typically about 0.1. The analysis of the velocity profiles shows that the maximum vorticity thickness, $\delta_u = \Delta U/(\partial u_x/\partial z)_{\max}$, ranged from 5 to 8 mm for all the experiments. Thus, the tank depth was always below $4.4\delta_u$, indicating that the horizontal boundaries may significantly affect the mixing properties of the flow.[21]

An example of the parallel shear layer prior to the onset of the instability is given in Fig. 2, where the vertical profiles of $\langle u_x\rangle$ (positive rightwards, see Fig. 1) and density $\langle\rho\rangle$ from Expt #5 of Table I are shown (this experiment is not further discussed since it did not return to the parallel-flow condition

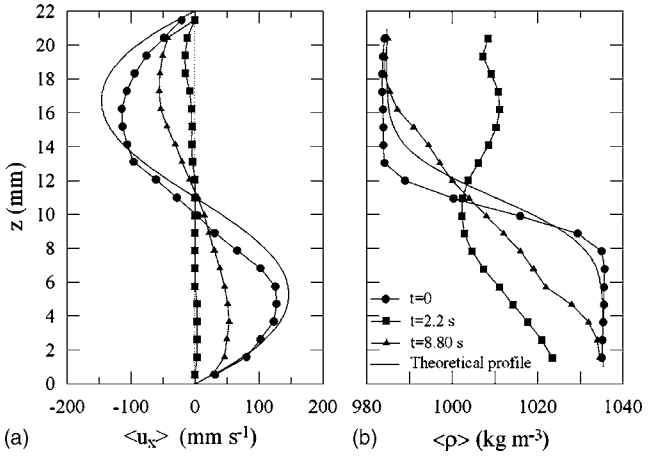

FIG. 2. Vertical profiles of the longitudinal velocity (a) and density (b) observed during the phase of parallel shear flow before the onset of the instability (circles), during the collapse of the KH billows (squares) and the phase of restratification (triangles) for Expt #5. The dotted lines indicate the theoretical profiles proposed in Refs. 22 [panel (a)] and 23 [panel (b)].

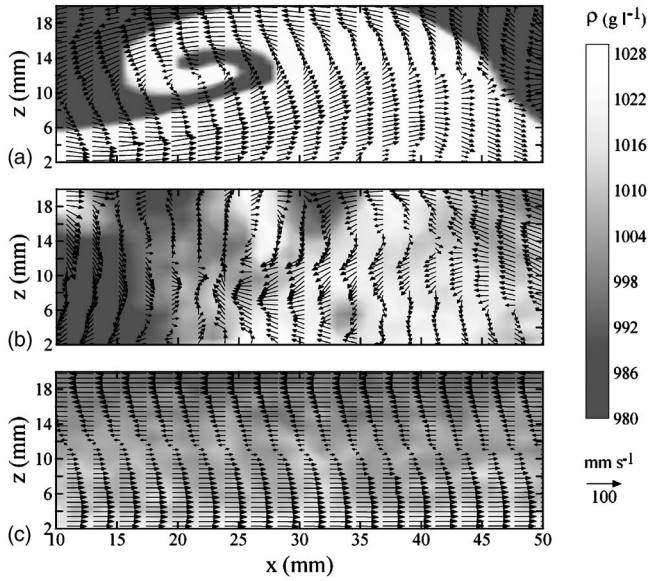

FIG. 3. Temporal evolution of the mass-density (map) and velocity (vectors) fields for Expt #5 during (a) the billow formation (t=0.8 s), (b) the billow collapse (t=1.8 s), and (c) the shear layer restratification (t=9.6 s). The time instant t=0 corresponds to the onset of the instability.

by the termination of the acquisition of the two cameras). Operator $\langle\cdot\rangle$ indicates longitudinal averaged variables computed over the wavelength λ of one of the KH billows lying in the frame area. The time origin t=0 corresponded to the onset of the instability, i.e., the instant the shear layer departed from the parallel flow condition. A simple analysis of the flow shows that at t=0 (line with circles) the gradient Richardson number was below 1/4 for all the experiments making the flow prone to the formation of KH billows. It is well-visible from the figure the large density variation occurring at the interface and the two velocity maxima located approximately at the half of the upper and the lower layer. There is reasonable agreement with theoretical velocity and density profiles found in the literature. In particular, the velocity profile in Fig. 2(a) (dotted line) represents the solution[22] of the Boussinesq equations written for a two-dimensional, stationary, stratified shear flow provided that $\rho(z)=1-\Delta'[\mathrm{erf}(\sigma z)/\mathrm{erf}(\sigma)]$ is the density profile [Fig. 2(b), dotted line]. The latter is the approximate solution of the Fick's diffusion equation proposed by Ref. 23, where $\Delta'=\Delta\rho/2\rho_0$, $\sigma=H/\sqrt{4\kappa_\rho\tau_0}$ is the diffusion parameter, $\sqrt{4\kappa_\rho\tau_0}$ is the magnitude of the propagation distance in time of the diffusive effects and erf() is the error function. (See Ref. 20 for a more detailed discussion; these authors also proposed a more generalized form for both the density and velocity profiles.) For the experiments considered in the present analysis, the time τ_0(≈30 min) corresponded to that necessary to assure the disappearance of all the disturbances which arose from the filling process before the tank was suddenly inclined.

C. The KH billow

The overall flow dynamics is well illustrated in Fig. 3, where the cross sections of the evolving velocity (vector) and

density (map in color levels) fields relative to three, representative, time instants taken during the experiment described above are shown. When the gradient Richardson number was smaller than 1/4 somewhere in the fluid an (two-dimensional) array of KH waves, with wavelength λ ranging from ~5 to ~6 cm, began to form at the density interface. The basic density profiles at $t=0$ show that the dimensionless wave number $\alpha=2\pi/(\lambda/\delta_\rho)$ was about 3 independent on the bulk Richardson number. Here, $\delta_\rho=\Delta\rho/(\partial\rho/\partial z)_{\max}$ is the maximum density gradient thickness. This is consistent with the laboratory results of Ref. 12, who found $\alpha=3$, on average.

The KH waves continued to grow in amplitude reaching a stage in which some lighter fluid was rolled under denser fluid and vice versa, resulting in patches of static instability [panel (a)]. This caused each wave to collapse, producing isolated spots of turbulence [panel (b)] which mixed the two fluids. Density and momentum were transferred between the fluids reducing the shear between the layers, as reflected by the velocity and density profiles reported in Fig. 2 (lines with squares). The turbulence then decayed and the remaining patches of homogeneous fluid tended to reorder according to their density, causing the partial restratification of the flow [panel (c)]. As time elapsed, viscous effects gained importance over inertial ones, and damped out small scale fluctuations with a progressive relaminarization of the flow.

By comparing the magnitude of the velocity and density fields prior to (circles in Fig. 2) and after the KH billows collapse (triangles) it is apparent that the flow lost part of its kinetic energy while, at the same time, increased its potential energy. This is an intrinsic characteristic of mixing in stably stratified flows as long as heavy fluid raised and light fluid lowered through mixing. The ratio of the potential energy increase to the kinetic energy lost during the event gives a quantitative measure of the efficiency of mixing. Questions related to this topic will be addressed in details at the end of the next subsection.

From the experiments, we calculated a series of quantities describing the flow field at the middle of the tank height ($z=H$). In particular, Fig. 4 shows the temporal evolution of the mean squared buoyancy frequency, $\langle N^2\rangle$, the mean velocity shear $\langle\partial u_x/\partial z\rangle$, and the gradient Richardson number $\langle \mathrm{Ri}_G\rangle$ for Expt #2 [Figs. 4(a)–4(c), respectively]. As expected, at $t=0$ the flow (initially laminar) was characterized by values of $\langle \mathrm{Ri}_G\rangle$ below the linear stability limit 1/4 [Fig. 4(c), dashed line].

Inspection of Fig. 4 suggests that 3 different flow regimes could be identified, that will be indicated by A, B, and C. During regime A both $\langle N^2\rangle$ and $\langle\partial u_x/\partial z\rangle$ rapidly decreased in magnitude as a result of the interface deformation during the rolling up of the billows. This phase was followed by the collapse of the billows ($t\cong 3.2$ s) which promoted turbulence and associated vertical transport and mixing of both mass and momentum throughout the channel (B). This stage of the flow was signified by intense oscillations around zero of $\langle\partial u_x/\partial z\rangle$ and by small (positive) $\langle N^2\rangle$. Also, $\langle \mathrm{Ri}_G\rangle$ remained positive [Fig. 4(c)] with the exclusion of sporadic bursts of

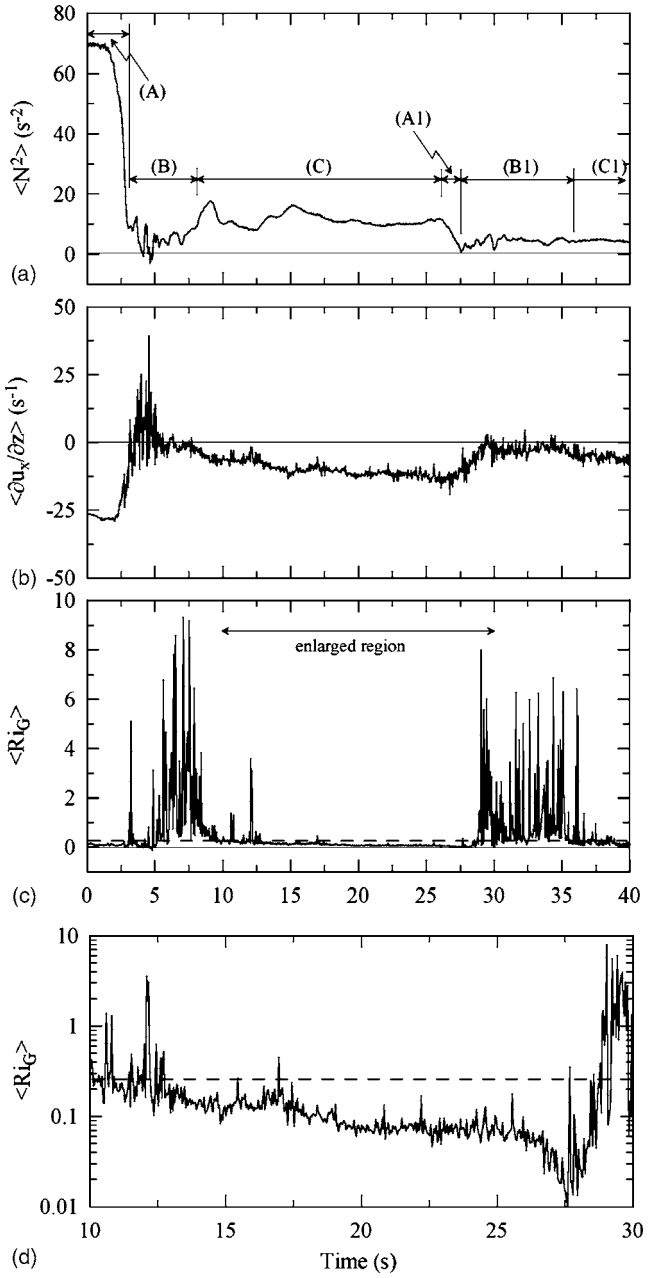

FIG. 4. Temporal evolution of quantities calculated at the middle of the tank for Expt #2. (a) Square of the buoyancy frequency $\langle N^2\rangle$, (b) longitudinal velocity shear $\langle\partial u_x/\partial z\rangle$, (c) gradient Richardson number $\langle \mathrm{Ri}_G\rangle$, and (d) enlarged region of plot (c). The time instant $t=0$ corresponds to the onset of the instability, while the dashed line in (c) and (d) indicates $\mathrm{Ri}_G=1/4$.

negative values associated with negative $\langle N^2\rangle$ [Fig. 4(a)] as a consequence of the overturning of the interfacial layer (statically unstable density distribution).

As both Figs. 4(a) and 4(b) indicate, at $t\cong 8.3$ s$\langle\partial u_x/\partial z\rangle$ started to increase substantially in magnitude, while $\langle N^2\rangle$ oscillated slowly around $\cong 10$ s^{-2} (regime C) as a result of the flow relaminarization induced by the stable stratification. Furthermore, the rise of $\langle\partial u_x/\partial z\rangle$ caused $\langle \mathrm{Ri}_G\rangle$ to fall more and more below the critical value 1/4 [see the expanded view of Fig. 4(c) replotted in Fig. 4(d)], paving the way to the onset of a second series of KH instabilities at $t\cong 26$ s occurring at the (now more diffuse) sheared density

interface. As for the first series, three dynamical regimes could be recognized within the life cycle of the billows (indicated by A1, B1, and C1). The first stage (A1) was analogous to the above-described regime A, while the ensuing stage (B1) represented the counterpart of regime B and characterized the KH billows collapse. Although the KH billowing was not as intense as that observed in regime B, it was strong enough to mix further the two fluids. A possible reason for this disparity was the stronger confinement of the KH billows during the latter regime due to the larger bulk Richardson number characterizing the second series. In fact, since the small-scale structures responsible for mixing extract their energy from the KH billow, if the billow cannot fully develop the intensity of mixing may be significantly reduced.

Finally, during regime C1 the flow evolved rather similarly to regime C and tended again toward the laminar state. Note that the turbulent activity after the collapse of the KH billows at $z=H$ subsided earlier for the first series of billows than for the second one (compare the time duration of regimes B and B1) due to the weaker density stratification at $z=H$ occurring in the latter case.

The sequence of events described above (three dynamical regimes occurring twice during each experiment, for a total of six stages) was common to all of the experiments reported in Table I. Careful inspection of the videotape records of the experiments showed that the flow was not affected by the surges from the channel ends during the time period considered in the analysis. This can also be seen from Fig. 4 and is further confirmed by numerical analysis conducted by Ref. 20. These authors, in fact, showed that for the adopted values of the flow parameters the return surges from the ends of the tank arrive at the middle of the tank normally at $t=50$ s.

D. Analysis of mixing

1. Flow energy and efficiency of mixing

It is well known that the background or minimum potential energy E_b, viz.,

$$E_b = \frac{1}{\lambda 2H}\int_0^{2H}\int_0^{\lambda} g\rho_b z \mathrm{d}x\mathrm{d}z \tag{4}$$

is a key parameter with which to quantify mixing in a stably stratified flow characterized by macroscopic fluid motion. Here, $\rho_b(z)$ is the stable density profile introduced by Thorpe,[24] obtained by rearranging the actual density profile into a monotonically varying density profile with minimum potential energy. Note that (4) is an appropriate two-dimensional version of the volume-averaged background potential energy associated with the flow field. The importance of the background potential energy lies in the fact that it represents the fraction of potential energy resulting from the irreversible process of mixing. The difference between the total potential energy of the flow,

$$E_p = \frac{1}{\lambda 2H}\int_0^{2H}\int_0^{\lambda} g\rho z \mathrm{d}x\mathrm{d}z \tag{5}$$

and E_b gives the available potential energy $E_a=E_p-E_b$, i.e., the fraction of potential energy that can be reversibly converted into kinetic energy. That difference explains the nature of the flow. During the roll-up and collapse of the KH waves some heavy fluid was advected upwards and, at the same time, some light fluid moved downward. However, large coherent patches of fluid resulted from the advection governed by the large scale structures (stirring) at the end of the wave collapse. They were able to reorder again according to their density and did not contribute to mixing, whereas the small scale motions gave the main contribution to the mixing and to the increase in the background potential energy.

A theoretical estimation of the rate of change of the background potential energy was given by Ref. 19, which quantified the rate at which a scalar mixes in a fluid in terms of the scalar flux across isoscalar surfaces. They found that, in the absence of advective and diffusive mass fluxes across the boundaries, its rate of change is equal to the diapycnal flux, Φ_d,

$$\mathrm{d}E_b/\mathrm{d}t = \Phi_d, \tag{6}$$

namely, Φ_d represents the flux of density across constant density surfaces,

$$\Phi_d = -\frac{\kappa_\rho g}{2H}\int_0^{2H}\frac{\langle|\nabla\rho|^2\rangle_{\mathrm{iso}}}{\mathrm{d}\rho_b/\mathrm{d}z}\mathrm{d}z, \tag{7}$$

where $\langle\cdot\rangle_{\mathrm{iso}}$ indicates an average over an isopycnal surface. Note that Φ_d is a positive quantity since the vertical gradient of the Thorpe's profile $\rho_b(z)$ is always negative. The method derived by Ref. 19 has been applied successfully in several numerical studies (e.g., Refs. 25 and 28), whereas, to the extent of the knowledge of the authors, Eq. (7) has never been used for the estimation of the diapycnal flux from experimental data.

The assessment of the efficiency characterizing mixing processes is also of crucial interest in stratified flow investigations. Numerous studies have concentrated on estimating mixing efficiency utilizing different definitions.[26–30] In the present study we shall apply the definition of mixing efficiency (also known as the flux Richardson number Rf) as used by Refs. 26 and 27, namely, the amount of energy gained per unit time via the mixing process associated with density fluctuations, $\Phi_d-\Phi_i$, relative to the total dissipation rate of kinetic energy, viz.,

$$\mathrm{Rf} = \frac{\Phi_d-\Phi_i}{\Phi_d-\Phi_i+\varepsilon}. \tag{8}$$

Here, ε is the dissipation rate of turbulent kinetic energy, while $\Phi_i=\kappa_\rho g\Delta\rho/2H$ accounts for the potential energy production by molecular diffusion which would occur if the fluid was at rest. Although this term is generally negligible compared to the mixing contribution of Φ_d it can become important in the case of weak turbulence.[26,30] The quantity $\Phi_d-\Phi_i$ therefore assumes the meaning of fluctuating diapycnal diffusivity.

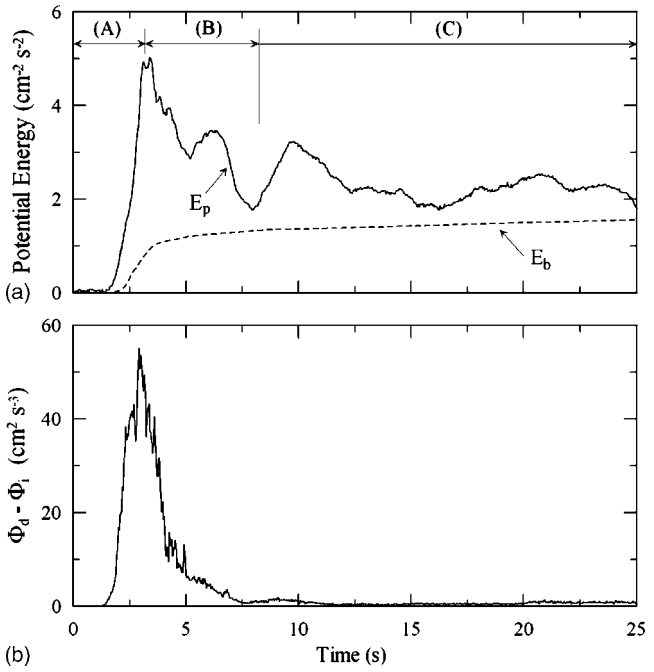

FIG. 5. (a) Temporal evolution of the total potential energy E_p as given in (5) (continuous line) and the background potential energy E_b (4) (dashed line) for Expt #2. The distance between the curves represents the available potential energy $E_a=E_p-E_b$. (b) Temporal evolution of the fluctuating diapycnal diffusivity $\Phi_d-\Phi_i$.

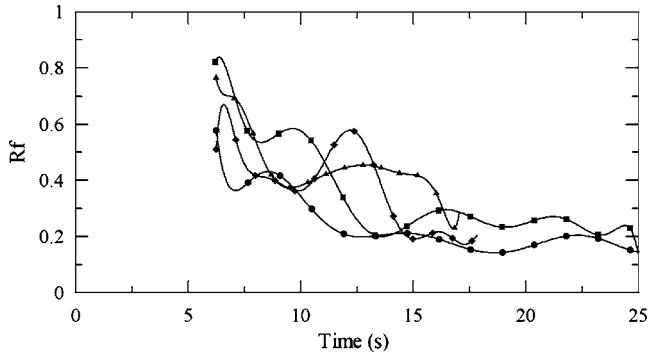

FIG. 6. Temporal evolution of the mixing efficiency Rf for Expt #1 (line with circles), Expt #2 (squares), Expt #3 (diamonds), and Expt #4 (triangles). Note that Expt #4 was not continued to its asymptotic state.

Since only two velocity components were measured in the present experiment, the approximation valid for isotropic turbulence was used to evaluate the dissipation rate,[31]

$$\varepsilon = \frac{15}{4}\nu\left[\left(\frac{\partial u_x'}{\partial z}\right)^2 + \left(\frac{\partial u_z'}{\partial z}\right)^2\right]. \tag{9}$$

That must be considered a rough estimate since the buoyancy Reynolds number, $R_b=\varepsilon/\nu N^2$, in our experiments is order of one, and therefore did not satisfy the requirement $R_b>20$ found by Yamazaki and Osborne[32] for the applicability of Eq. (9).

The background (E_b, dashed line) and the total (E_p, continuous line) potential energies referred to in Expt #2 (the same investigated in Fig. 4) are plotted versus time in Fig. 5(a). After the onset of the instabilities E_p increased because heavy fluid rose upwards during the KH instability growth, reaching a maximum close to the state of saturation of the KH billows occurring at $t\cong 3.2$ s. The onset of the instabilities also coincided with the variation in the background potential energy E_b, and its growth was initially slower compared with E_p. The collapse of the KH billows led to a rapid decrease in E_p followed by strong oscillations due to large scale motions (stage B). During this stage E_b was considerably lower then E_p and grew monotonically toward E_p. After, the flow was dominated mainly by buoyancy and was characterized by rapid relaminarization and slow oscillations of E_p around a nearly constant value as a result of the wavy motion which followed the billow collapse (stage C). Obviously, those oscillations were totally absent in the time evolution of E_b because of the procedure of Thorpe reordering in which the evaluation of E_b was based. It also appears that E_b reached a maximum rate of growth at $t\cong 2.9$ s. As is apparent in the time evolution of $\Phi_d-\Phi_i$ shown in Fig. 5(b), that was strictly related to the maximum in $\Phi_d-\Phi_i$ [cf. also (6)]. The figure also shows that $\Phi_d-\Phi_i$ attained a minimum at $t\cong 12$ s, which was maintained throughout the remainder of stage C. This behavior is consistent with the linear growth in time exhibited by E_b during the stage C and is also in qualitative agreement with the numerical results reported in Refs. 26, 27, and 30.

The maximum rate of growth of E_b occurred at about $t\cong 2.9$ s [Fig. 5(a)], thus before both the transition to turbulence and occurrence of the maximum value of E_p. Similarly, the time evolution of $\Phi_d-\Phi_i$ exhibited an absolute maximum before the KH instability saturated. These last two results contrast with the previous finding of other researchers including Refs. 26, 27, and 30, which observed the maximum in the diapycnal flux during the turbulent stage following the collapse of the KH billow. A possible reason for this discrepancy lies in the spatial resolution used to measure the density, not sufficient to detect the smallest mixing scales of the flow.

The features described above also occur during the three stages A1–C1 of the second series of KH billows, even if the changes observed both in total and in background potential energies are much lower than the ones reached during the first series A–C, characterized by stronger mixing.

The above mentioned discrepancies characterizing the evaluation of the diapycnal flux during the stages A and B, have suggested restricting our analysis of the mixing efficiency only beyond the billow collapse ($t>7$ s). Figure 6 shows the time variation of the mixing efficiency Rf for the experiments reported in Table I. Shortly after the transition to turbulence Rf was still large in all the analyzed cases, in consonance with the numerical findings of Ref. 26. She also found that the maximum Rf occurred before the billow collapse, when the flow was still laminar and only little dissipation of KE was associated with the billows. Similar considerations apply for the numerical experiments reported in Ref. 30, even though they considered the so-called "flux coefficient" $\Gamma_i=(dE_b/dt-\Phi_i)/\varepsilon$ instead of Rf as a proxy for the mixing efficiency. In essence, after the billow collapse the turbulence irreversibly mixes the fluid through small-scale structures, but this mixing is less efficient compared to that

occurring during the preturbulent phase due to the larger turbulent kinetic energy consumption associated with the small (highly dissipative) scales that dominated the flow.

Figure 6 also shows that the mixing efficiency exhibits an asymptote for large times in Expt #1, Expt #2, and Expt #3 close to 0.2, in consonance with the numerical results obtained by other authors.[26,27,33] Given that these three experiments referred to different Re (cf. Table I), the asymptote of Rf is plausibly independent of the initial Reynolds number, at least over the range of Reynolds number investigated here. Note that a general independence of the asymptotic value of the flux coefficient from the initial Reynolds number was also numerically predicted by Ref. 30. It is also apparent the absence of any significant dependence of Rf on the bulk Richardson number. Because in Expt #4 the development of the flow was not followed for a time sufficiently long to achieve the asymptotic state due to the onset of the second series of KH at nearly 18 s, we can only speculate that the mentioned insensitiveness were also valid for the latter experiment.

2. Eddy diffusivities of mass and momentum

As mentioned in the Introduction, the experimental apparatus being employed is suited to the simultaneous measurements of velocity and density fields. Therefore, since one of the goals of turbulent mixing studies is the parameterizations of turbulent diffusivities, the present laboratory data have been used to calculate the eddy diffusivity of momentum

$$\langle K_M \rangle = -\frac{\langle u_x' u_z' \rangle}{\langle \partial u_x / \partial z \rangle} \tag{10a}$$

and mass

$$\langle K_\rho \rangle = -\frac{\langle u_z' \rho' \rangle}{\langle \partial \rho / \partial z \rangle} \tag{10b}$$

as a function of the gradient Richardson number $\langle \mathrm{Ri}_G \rangle$. Both of the eddy diffusivities were estimated using the data collected during the regimes C and C1 [see Fig. 4(a)], where the vertical profiles of the mean horizontal velocity and density varied smoothly and definitions (10a) and (10b) apply.[26] Also, during regimes C and C1 the reversible effects of stirring should be of little importance. This fact is crucial for the evaluation of mixing in that the instantaneous values of the vertical fluxes may be influenced by (unwanted) effects associated with stirring.

The dependence of $\langle K_M \rangle$ and $\langle K_\rho \rangle$ upon $\langle \mathrm{Ri}_G \rangle$ is illustrated in Fig. 7. In the $\langle \mathrm{Ri}_G \rangle$ range of the current experiments both $\langle K_M \rangle$ and $\langle K_\rho \rangle$ were larger than their molecular diffusive counterparts ($\nu \approx 10^{-2}$ and $\kappa_\rho \approx 10^{-5}$ cm^2 s^{-1}, respectively), even though $\langle K_M \rangle$ tended to drop to ν at large $\langle \mathrm{Ri}_G \rangle$. This is not surprising, given that during the regimes C and C1 the flow relaxed toward a regime of quasihorizontal motions and decaying turbulent activity.

Figure 7 also shows the dependence of $\langle K_\rho / K_M \rangle$, i.e., the inverse of the turbulent Schmidt number, on $\langle \mathrm{Ri}_G \rangle$. It is apparent that $\langle K_\rho / K_M \rangle$ was nearly equal to unity (as in the neutral case) for $\langle \mathrm{Ri}_G \rangle$ less than ~0.2. Then, it seems to show a slight decrease with increasing $\langle \mathrm{Ri}_G \rangle$ when the latter was below ~0.4. This behavior is consistent with the results presented in Ref. 34 based on a laboratory study of stably stratified shear flow (see open triangles in Fig. 7) and with other numerical studies regarding similar topics (see Ref. 35, and references therein). For stronger stratification it was found an increase in $\langle K_\rho / K_M \rangle$, in disagreement with the results from the authors mentioned above. However, given the small number of data points subjected to statistical averaging, for $\langle \mathrm{Ri}_G \rangle$ greater than 0.5 the results must be considered with circumspection. Finally, it is noteworthy the resemblance of the laboratory experimental data presented above to the relationship for the inverse of the turbulent Prandtl number $\mathrm{Pr}^{-1} = K_H / K_M$ (K_H is the eddy diffusivity for heat) suggested by Mahrt and Vickers[36] using atmospheric measurements (dashed line), viz., $\mathrm{Pr} = 1 + 3.7\mathrm{Ri}_G$. It is of note that the large difference between the Prandtl number for air (~0.7) and the Schmidt number in the shear flow considered here (~700) did not play any significant role, at least for the range of $\langle \mathrm{Ri}_G \rangle$ investigated here.

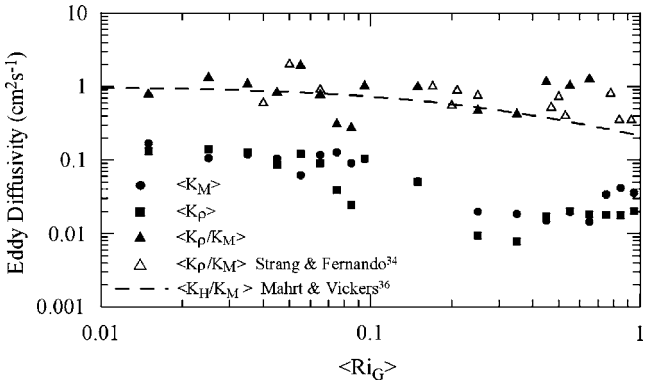

FIG. 7. Eddy diffusivity of momentum $\langle K_M \rangle$, eddy diffusivity of mass $\langle K_\rho \rangle$, and the ratio $\langle K_\rho / K_M \rangle$ as a function of $\langle \mathrm{Ri}_G \rangle$. Also included are the laboratory data given by Strang and Fernando (Ref. 34) and the relationship proposed by Mahrt and Vickers (Ref. 36) based on atmospheric field experiments (dashed line).

IV. CONCLUSIONS

Simultaneous, whole field measurements of velocity and density were employed to experimentally investigate a vertical plane in the mixing of a stratified, parallel shear flow as it evolved during the lifetime of a Kelvin-Helmholtz (KH) billow. The different stages of the KH billow, that is, its growth, its collapse, and the subsequent relaxation of the flow toward a state of decaying stably stratified turbulence were examined and discussed.

We also provided here an estimation of the efficiency of mixing Rf. The diffusive flux of density responsible for mixing was evaluated making use of the method proposed by Winters *et al.*[18,19] To our knowledge, this is the first time this has been done through laboratory experiments. The results showed a qualitative agreement with the direct numerical simulations performed by Staquet,[26] particularly during the stage of relaxation, when an asymptote close to the canonical value of 0.2 was found for Rf. We have shown that for the

experimental conditions considered in the present paper, the asymptotic value reached by Rf was independent of the bulk Richardson number and of the initial Reynolds number, in agreement with the numerical results presented by other researchers. It has also been shown that the eddy diffusivities of density and momentum as a function of the stability expressed in terms of the gradient Richardson number were in reasonable agreement with those obtained by other researchers both in laboratory experiments and observational data in atmospheric stably stratified flows.

Despite some constraints of the laboratory model, the information we gave here provided observational evidence for a number of key features of KH billows which form in natural geophysical flows.

ACKNOWLEDGMENTS

The authors would like to thank Professor L. D'Alpaos, Professor A. Defina, Dr. S. Lanzoni, and Dr. F. M. Susin that designed and constructed the tilting tank. The assistance of Dr. C. Accettola to the measurements and data analysis was greatly appreciated. In addition, we would like to thank Dr. G. Carnevale as well as two anonymous referees for the useful comments made on this paper, which led to substantial improvement of its content.

[1] J. D. Woods, "Wave-induced shear instability in the summer thermocline," J. Fluid Mech. **32**, 791 (1968).
[2] P. Monti, H. J. S. Fernando, M. Princevac, W. C. Chan, T. A. Kowalewski, and E. R. Pardyjak, "Observations of flow and turbulence in the nocturnal boundary layer over a slope," J. Atmos. Sci. **59**, 2513 (2002).
[3] W. R. Peltier and C. P. Caulfield, "Mixing efficiency in stratified shear flows," Annu. Rev. Fluid Mech. **35**, 135 (2003).
[4] I. P. D. De Silva, H. J. S. Fernando, F. Eaton, and D. Hebert, "Evolution of Kelvin-Helmholtz billows in nature and laboratory," Earth Planet. Sci. Lett. **143**, 217 (1996).
[5] C. Staquet and J. Sommeria, "Internal gravity waves: from instabilities to turbulence," Annu. Rev. Fluid Mech. **34**, 559 (2002).
[6] P. K. Kundu, *Fluid Mechanics* (Academic, San Diego, 1990).
[7] J. W. Miles, "On the stability of heterogeneous shear flows," J. Fluid Mech. **10**, 496 (1961).
[8] L. N. Howard, "Note on a paper of John W. Miles," J. Fluid Mech. **10**, 509 (1961).
[9] E. J. Strang and H. J. S. Fernando, "Entrainment and mixing in stratified shear flows," J. Fluid Mech. **428**, 349 (2001).
[10] E. R. Pardyjak, P. Monti, and H. J. S. Fernando, "Flux Richardson number measurements in stable atmospheric shear flows," J. Fluid Mech. **459**, 307 (2002).
[11] T. J. McDougall, "On the elimination of the refractive-index variations in turbulent density-stratified liquid flows," J. Fluid Mech. **93**, 83 (1979).
[12] B. Atsavapranee and M. Gharib, "Structures in stratified plane mixing layers and the effects of cross shear," J. Fluid Mech. **342**, 53 (1997).
[13] C. D. Troy and J. R. Koseff, "The generation and quantitative visualization of internal breaking waves," Exp. Fluids **38**, 549 (2005).
[14] G. Querzoli, "A Lagrangian study of particle dispersion in the unstable boundary layer," Atmos. Environ. **30**, 282 (1996).
[15] S. A. Thorpe, "A method of producing a shear flow in a stratified fluid," J. Fluid Mech. **32**, 693 (1968).
[16] P. F. Linden, "Mixing in stratified fluids," Geophys. Astrophys. Fluid Dyn. **13**, 3 (1979).
[17] H. J. S. Fernando, "Turbulent mixing in stratified fluids," Annu. Rev. Fluid Mech. **23**, 455 (1991).
[18] K. B. Winters, P. N. Lombard, J. J. Riley, and E. A. D'asaro, "Available potential energy and mixing in density-stratified fluids," J. Fluid Mech. **289**, 115 (1995).
[19] K. B. Winters, E. A. D'asaro, "Diascalar flux and the rate of fluid mixing," J. Fluid Mech. **317**, 179 (1996).
[20] A. Defina, S. Lanzoni, and F. M. Susin, "Stability of a stratified viscous shear flow in a tilted tube," Phys. Fluids **11**, 344 (1999).
[21] S. P. Haigh and G. A. Lawrence, "Symmetric and nonsymmetric Hölmböe instabilities in an inviscid flow," Phys. Fluids **11**, 1459 (1999).
[22] F. M. Susin, "Indagini teoriche e sperimentali sulla stabilità di un moto parallelo di fluido viscoso eterogeneo," Ph.D. dissertation, University of Padua, Italy, 1998 (in Italian).
[23] S. A. Thorpe, "Experiments on the instability of stratified shear flows: Miscible fluids," J. Fluid Mech. **46**, 299 (1971).
[24] S. A. Thorpe, "Turbulence and mixing in a Scottish loch," Philos. Trans. R. Soc. London, Ser. A **286**, 125 (1977).
[25] C. Staquet and K. B. Winters, "Mixing in a stably-stratified shear layer," in Proceedings of the XIth Symposium on Turbulent Shear Flows, edited by G. Binder, Vol. 2, pp. 25–30 (1997).
[26] C. Staquet, "Mixing in stably stratified shear layer: two- and three-dimensional numerical experiments," Fluid Dyn. Res. **27**, 367 (2000).
[27] C. Caulfield and W. Peltier, "Anatomy of the mixing transition in inhomogeneous and stratified free shear layers," J. Fluid Mech. **413**, 1 (2000).
[28] P. Bouruet-Aubertot, C. Koudella, C. Staquet, and K. B. Winters, "Particle dispersion and mixing by breaking internal gravity waves: Two-dimensional numerical experiments," Dyn. Atmos. Oceans **32**, 95 (2001).
[29] J. F. Scinocca, "The mixing of mass and momentum by Kelvin-Helmholtz billows," J. Atmos. Sci. **52**, 2509 (1995).
[30] W. D. Smyth, J. N. Moum, and D. R. Caldwell, "The efficiency of mixing in turbulent patches: Inferences from direct simulations and microstructure observations," J. Phys. Oceanogr. **31**, 1969 (2001).
[31] J. Hinze, *Turbulence* (McGraw-Hill, New York, 1975).
[32] H. Yamazaki and T. R. Osborne, "Dissipation estimates for stratified turbulence," J. Geophys. Res. **95**, 9739 (1990).
[33] W. D. Smyth and J. N. Moum, "Length scales of turbulence in stably stratified mixing layers," Phys. Fluids **12**, 1327 (2000).
[34] E. J. Strang and H. J. S. Fernando, "Vertical mixing and transport through a stratified shear layer," J. Phys. Oceanogr. **31**, 2026 (2001).
[35] V. Armenio and S. Sarkar, "An investigation of stably stratified turbulent channel flow using large-eddy simulation," J. Fluid Mech. **459**, 1 (2002).
[36] L. Mahrt and D. Vickers, "Formulation of turbulent fluxes in the stable boundary layer," J. Atmos. Sci. **60**, 2538 (2003).